Autonomic responses to proprioceptive and visual errors during single-trial reach adaptation

Motoko Nogami[1,2], Nobuhiro Hagura[1,2], Atsushi Yokoi[1,2]

1. Graduate School of Frontier Biosciences, Osaka University, Suita Japan
2. Center for Information and Neural Networks, Advanced ICT Research Institute, National Institute of Information and Communications Technology, Suita, Japan

Address for Correspondence:

Atsushi Yokoi (ayokoi@nict.go.jp)
Center for Information and Neural Networks,
Advanced ICT Research Institute,
National Institute of Information and Communications Technology
1-4 Yamadaoka, RM 2B6
Suita, Osaka 565-0871, Japan

Abstract

Recent evidence suggests that not only the implicit but also explicit cognitive learning processes play a significant role in acquiring sophisticated motor skills. How these processes interact with each other, or how we can quantify them without bias, are, however, still elusive. To tackle these issues, here we employ simultaneous measurement of peripheral autonomic signals during the short-term motor learning paradigm. Through extensive research in the cognitive learning field, autonomic measures, such as pupil diameter, have been shown to reflect various internal states associated with the adjustment of learning behavior, suggesting that they could also be an effective tool to assess cognitive processes during motor learning. In a series of experiments, we measured the multiple autonomic signals, including pupil diameter, skin conductance, and heart rate, while human participants of both sexes learned to reach under occasional proprioceptive or visual disturbances. We characterized the phasic autonomic responses to errors and evaluated their influence over motor learning, which was quantified by comparing the trials immediately before and after the error event. The results demonstrated the dose-dependent increase in the phasic autonomic responses to errors of both modalities, consistent with higher cognitive demand in large errors. Using a latent factor analysis, which combines the multimodal autonomic response data, we also found a statistical relationship between the latent autonomic states and the motor learning rate, the suppression of implicit motor adaptation at higher error-induced sympathetic state. These results provide a novel insight into how internal state change affects motor learning.

Introduction

Learning complex motor skills, such as throwing a 100 mph ball accurately into a strike zone or hitting that ball over the fence, is supported by a complex interplay between implicit and explicit (or cognitive) learning processes. Although a large focus of motor learning studies has been on the implicit learning process (Shadmehr et al., 2010; Wolpert et al., 2011), more recent studies have started emphasizing the importance of explicit (cognitive) processes in motor learning (Krakauer et al., 2019; Tsay et al., 2024). For example, when there is constant rightward wind and the ball one threw missed the target to the right, he/she may deliberately aim to the left in the next pitch (i.e., explicit re-aiming). At the same time, the implicit learning process gradually adjust the throwing movement to the left, as well, and it is generally thought that repeating this cycle may eventually converge to less reliance on the explicit re-aiming strategy with the adjusted implicit sensorimotor mapping. Interestingly, however, these implicit and explicit (cognitive) learning processes sometimes cooperate (Miyamoto et al., 2020), but other times compete (Mazzoni and Krakauer, 2006; Albert et al., 2022) with each other. Thus, while the wealth of behavioral evidence suggests that not only the implicit, but also explicit cognitive learning processes are essential for sophisticated motor behavior, it raised further questions, such as the detailed mechanism of the interplay between the two processes, what drives the explicit process, and how we quantify or dissociate the two processes without biasing the system (Maresch et al., 2021; ‘t Hart et al., 2024). To address these questions, we expect that the peripheral autonomic signals could provide a new insight into the explicit cognitive processes during motor learning.

Autonomic indices, such as pupil diameter or heart rate, have been frequently used in cognitive research fields to probe changes in various internal states during cognitive tasks, such as mental effort (Kahneman and Beatty, 1966; Ahern and Beatty, 1979) or surprise and uncertainty (Preuschoff et al., 2011; Nassar et al., 2012). Especially, pupil diameter is getting growing attention in cognitive neuroscience field for its relation to central noradrenergic nuclei, the locus coeruleus (LC) (Aston-Jones and Cohen, 2005; Joshi et al., 2016; Joshi and Gold, 2020). The LC and noradrenaline (NA) has been extensively studied in the context of prefrontal attention (Sara, 2009; Arnsten et al., 2012), cognitive flexibility (Aston-Jones et al., 1994; Bouret and Sara, 2004; McBurney-Lin et al., 2022), novelty of stimuli/environment (Hervé‐Minvielle and Sara, 1995; Vankov et al., 1995), and memory formation and consolidation (Sara and Devauges, 1988; Sara et al., 1999; Strange et al., 2003; Takeuchi et al., 2016; Clewett et al., 2018, 2020). For instance, LC neurons increase their firing activity, similarly to the increase in reaction time, when animals adapt to the reversal in cue-reward contingency (Aston-Jones et al., 1997, 2000), and increase in baseline pupil diameter precedes the exploratory behavior when humans do the similar tasks (Gilzenrat et al., 2010; Jepma and Nieuwenhuis, 2011). These body of research, therefore, suggest that the autonomic indices and LC-NA system could also be a relevant source of information for motor learning with respect to the explicit cognitive processes. However, so far, surprisingly few numbers of studies have explicitly studied the autonomic activity or

LC-NA system during motor learning (White and French, 2016; Yokoi and Weiler, 2022).

Therefore, to gain basic insights about how autonomic activity changes during motor learning, we investigated the multiple sources of autonomic activity, including pupil diameter, skin conductance, and heart rate, in reaching paradigm. Specifically, we assessed the phasic response of these autonomic indices to various sizes of unexpected movement error applied either proprioceptively or visually. We further examined the relationship between the autonomic responses and learning rate (i.e., sensitivity to errors) which was quantified by comparing the trials immediately before and after the error event. The results demonstrated the dose-dependent increase in the phasic autonomic responses (pupil dilation, skin conductance response, and heart rate deceleration) in response to errors of both modalities. Using a latent factor analysis which combines the multimodal autonomic response data, we also found statistical relationship between the latent autonomic states and the motor learning rate. Our results suggest the possible mediation of error-driven autonomic state (or LC-NA activity) change in the adjustment of motor learning rate which might also be associated with the involvement of the explicit cognitive processes for large detectable errors.

Materials & Methods

Participants

Eighty-five human volunteers (58 men and 27 women, aged 19-31 years old) participated in this study. Participants in Experiment 1 consisted of 41 individuals, while those in Experiment 2 consisted of 44. All participants were right-handed verified with Flanders Handedness Questionnaire and no history of neurological disorders. Participants provided written informed consent before taking part in the study. The experimental protocols were approved by the ethical committees of the National Institute for Information and Communications Technology. Sample size per an experiment was based on a previous study collecting multiple autonomic indices (de Berker et al., 2016).

Apparatus

Participants sat in front of an LCD monitor and grasped the handle of a robotic manipulandum (Phantom Premium HF 1.5, 3D Systems, Inc.) with their right hand while resting their chin on a chin rest positioned in front of the monitor. An eye tracker (EyeLink 1000, SR Research Inc., Ontario, Canada) was placed under the monitor and measured the participants' pupil diameter (Fig. 1A). The chin rest and monitor were 44 cm apart. The coordinate for visual stimuli (start and target positions and a cursor representing the hand position) were in the x-y plane, while the handle motion was constrained in the x-z plane (Fig. 1A). The colors of the visual objects were adjusted to have approximately equal luminance to avoid changes in pupil diameter induced by the task stimuli (Yokoi and Weiler, 2022). Participants were unable to see their hand directly.

Electrocardiography (ECG) and skin conductance level (SCL) were measured by using the

BIOPAC system (BIOPAC MP160, BIOPAC SYSTEMS Inc.). ECG electrodes were placed at three points on the trunk (below the right clavicle, below the left clavicle, and on the left rib). SCL electrodes were attached to the middle and index fingers of the left hand. For an additional index, photoplethysmography (PPG) was collected for 19 participants in Exp 1 and 29 participants in Exp 2. The pulse-oximeter sensor was attached to the left ring finger. The PPG data was not analyzed for this study due to the insufficient sample size compared to other autonomic signals.

Procedure

Participants were instructed to move a cursor (a white 5mm diameter dot) as straight as possible from a starting position (a gray 16mm diameter dot) to the center of a target (a gray 16mm diameter dot). After moving the cursor, they were asked to maintain the cursor on the target until the trial end (Fig. 1A). The home position and the target were 10cm apart. We instructed the participants to always aim straight at the target. Participants were required to minimize movement of their face to keep their gaze fixed on the target. They were also asked to keep their left hand still and suppress the blink during the movement to reduce noise for the SCR and the pupil measurement. A single trial progressed as follows. A trial started after a stable fixation and center hold was maintained for 1.0 sec. This was followed by a random delay of 1500-1900 msec, and then a go cue was provided as the target color turned into green. In the experiment, movement onset and offset were defined as the time points at which the speed of the handle exceeded 3.5 cm/sec and fell below 0.1 cm/sec, respectively. Movements that took longer than 1.5 sec to complete were warned by a visual message 'Too Slow!'. After the movement offset, endpoint feedback was provided for 3.0 sec. This feedback duration was chosen to reliably measure the skin conductance response to movement errors, which typically peaks around 1.5 to 3.0 sec from an event (Dawson et al., 2007). After the feedback period, the handle of the manipulandum automatically returned to the start position and the trial ended.

In order to accurately measure the autonomic error responses and the error-dependent change in reaching behavior (i.e., learning), we employed the single-trial learning paradigm with varying sizes of movement error (Marko et al., 2012; Kasuga et al., 2013; Hayashi et al., 2020). After every 4-6 trials of normal reaching movements without perturbations, a set of 3 trials was introduced to assess the single-trial motor adaptation. This "triplet" consisted of 2 probe trials and 1 perturbation trial placed in between. By comparing the motor outputs before and after the perturbation trial, the learning induced by the perturbation was quantified. The size of perturbation was randomly chosen from the set $p = \{\pm45, \pm30, \pm10, \pm5, 0^{\circ}\}$. Details about the perturbation and the assessment of motor output are described for each experiment below.

Before the main session, participants conducted 2 practice blocks with continuous cursor feedback (30 trials each) in the absence of any perturbations. Main experiment consisted of 7 blocks, each containing 72 trials. A 1-minute break was given after each block. After the third block a 5-minute

break was provided. After the main experiment, pupil calibration was performed by changing the background color of the monitor from light blue to either white (high luminance) or black (low luminance). This triggered the pupil light reflex, allowing the measurement of each participant's minimum and maximum pupil size in the current experimental environment. The range of pupil sizes was then used to normalize the pupil data within each participant, ensuring the data could be interpreted consistently across participants (Yokoi & Weiler, 2022).

Experiment 1 (proprioceptive error)

In Exp 1, 41 participants were recruited. Two participants were excluded from the analysis due to technical failure to measure either pupil or SCL/ECG data. As a result, the data for 39 participants were submitted for further analysis (age [mean±SD]: 22.5±2.65; sex: 27 male, 12 females; handedness score [mean±SD]: 9.74±0.60). In the Exp 1, we assessed pupil/autonomic responses to proprioceptive errors. Proprioceptive errors during reaching were induced by constraining the hand trajectory to a specific direction (chosen from ±45, ±30, ±10, ±5, or 0º) by using a force channel method (Scheidt et al., 2000; Hayashi et al., 2020) which mechanically constrains the handle trajectory (Fig. 1B). Similarly, motor output before and after the perturbation trial were measured by the force channel directed straight to the target (Fig. 1B; 0 deg). The channel stiffness and viscosity were 23 (N/cm) and 0.2 [N/(cms^{-1})], respectively. In the Exp 1, no online cursor feedback but only the endpoint feedback was provided. For the perturbation trials, endpoint feedback was also absent to minimize visual-proprioceptive discrepancy (i.e., visual error).

Experiment 2 (visual error)

In Exp 2, 44 participants were recruited. Of those, the data for 5 participants were removed from the analysis due to technical failure to measure either pupil or SCL/ECG signal. As a result, the data for 39 participants were submitted for further analysis (age: 22.1±2.16; sex: 28 male, 11 females; handedness: 9.69±0.95). In the Exp 2, we assessed pupil/autonomic responses to visuomotor errors. To this end, we provided both online and endpoint cursor feedback (a magenta dot of 7.5 mm diameter) for this experiment. Force channel was not used in entire experiment. Visuomotor errors were applied by rotating the cursor trajectory to a specific direction (chosen from ±45, ±30, ±10, ±5, or 0º) (Fig. 1C). For the consistency with the Exp 1, endpoint feedback was not provided in the perturbation trials. While both the online and endpoint feedback were not provided for the post-perturbation trials, they were provided for the pre-perturbation trials. This is to keep the participants unprepared to perturbations.

Data analysis

All analyses were conducted using custom-written codes with MATLAB R2015b (Mathworks, Natick,

MA, USA). For all the experiments, the data from the manipulandum (x-z positions, x-z velocities, and x-z command forces for the manipulandum handle) and the data from the eyetracker (x-y gaze positions and pupil diameter) were sampled at 200 Hz. Other autonomic data (ECG, SCL, and PPG) were sampled at 1000 Hz.

Kinematic data. The kinematic data for arm reaching were first smoothed with a Gaussian kernel of 35 ms full width half maximum (FWHM). Movement onset was re-defined as the point when the hand movement velocity first exceeded a threshold (10% of the peak velocity) at each trial. Similarly, movement offset was defined as the point when the hand movement velocity first fell below the threshold after movement onset.

To assess the single-trial error-dependent change in motor output and the sensitivity to errors (i.e., learning rate), we employed the following equations;

$$\delta(p)^i = O_{post}(p)^i - O_{pre}(p)^i, \tag{1}$$

$$LR(p) = \frac{\text{median}\left[\delta(p)^i\right]}{\text{median}[e(p)^i]}, \tag{2}$$

where the $\delta(p)^i$ represents the change in motor output (i.e., across-trial correction) at the *i*-th experimental block (*i* = 1, 2, …, 7) with the perturbation condition p (p = {±45, ±30, ±10, ±5, 0º }). Similarly, the $O_{post}(p)^i$ and the $O_{pre}(p)^i$ represent the motor output for post- and pre-perturbation trials at the *i*-th experimental block with the perturbation condition p, respectively. The $LR(p)$ represents the single-trial learning rate (sensitivity to errors) and the $e(p)^i$ represents the motor error for the perturbation condition p at the *i*-th block.

For Exp 1, similar to Hayashi et al. (2020) (Hayashi et al., 2020), we employed the force impulse for the O_{pre}, and O_{post} in Eq. 1. The impulse values were defined as the time integral of lateral force applied to the channel wall from the movement onset to the time of peak velocity, at the pre- and post-perturbation trials, respectively. Similarly, we used the force impulse at the perturbation trial as an index for proprioceptive error (e in Eq. 2). The single-trial learning rate (error sensitivity) was further calculated as the median of across-trial correction for all blocks divided by the median of proprioceptive errors for all blocks, respectively for each perturbation size (Eq. 2). For Exp 2, we used the hand movement angle for the O_{pre}, and O_{post} in Eq. 1. This was defined as the angle relative to the target direction, calculated at time of peak velocity, T_{peak};

$$\theta_{hand} = \text{atan}\left(\frac{x(T_{peak})}{y(T_{peak})}\right), \tag{3}$$

where the *x*(•) and *y*(•) represent the *x*- and *y*-position of the handle relative to the starting position. For the visuomotor error (e in Eq. 2), we used the angular deviation of the cursor relative to the target direction (i.e., hand angle + rotation angle). The rotation angle was randomly chosen from p = {±45, ±30, ±10, ±5, 0º}, similarly to Exp 1. The single-trial learning rate (error sensitivity) was similarly calculated as the median of across-trial correction for all blocks divided by the median of visuomotor

errors for all blocks, respectively for each perturbation size (Eq. 2).

Eyetracker data. For all the experiments, the gaze position and pupil (x-y gaze position and pupil diameter) data were preprocessed in the following way. First, we discarded data around each blink event, from 100 ms prior and up to 150 ms after the blink. We then interpolated over the discarded data using a piecewise cubic Hermite interpolating polynomial (Matlab interp1.m function with "pchip" option). After the interpolation, the gaze position data were smoothed by a second-order Savitzky-Golay filter with a frame length of 55 ms (sgolayfilt.m function). The eye velocities were then derived from the filter results. We employed 30 °/sec as the velocity threshold for saccade detection. For the pupil diameter data, to remove high-frequency noise, we smoothed the data with a Gaussian kernel with 235 ms FWHM. Furthermore, we individually normalized the pupil diameter data relative to the minima and maxima of the pupil diameter data measured during the light reflex trials. The normalized pupil diameter data were submitted for the further analyses.

We defined the tonic component of pupil changes as the pupil diameter measured before the go-cue presentation. We also defined the phasic pupil response to errors as the pupil dilation velocity after movement onset. The pupil dilation velocity was derived through the numerical derivative (diff.m function). Then, the trial-by-trial summaries of these pupil-related variables were defined as follows. The tonic baseline pupil diameter was defined as the average pupil diameter during the waiting period before the onset of the go-cue. The trial-by-trial phasic pupil responses to errors were defined as the average of the pupil dilation velocity within temporal regions of interest (ROIs) where the significant cluster of perturbation size was detected (Table 1 and 3, Small vs. Large). This was assessed by comparing the average time series of the pupil dilation velocity at the perturbation trials for the small ($|p| \leq 10°$) against the large ($|p| \geq 30°$) errors by the cluster-based permutation test (Maris and Oostenveld, 2007).

BIOPAC data. The SCL data were first filtered with the Second-order Savitzky-Golay filter with window size 300 ms. We then defined the skin-conductance response (SCR) as the numerical derivative of the SCL data, which was estimated through the Savitzky-Golay filter. Then the both of the SCL and the SCR data were downsampled to 200 Hz for further analyses.

The ECG data were filtered with the third-order Savitzky-Golay filter with window size 30 ms, and the time derivative of the filtered ECG data were estimated through the filter result. These data were then used to detect the timing of R-wave peaks. We then estimated the instantaneous R-R intervals as the following equations.

$$RRI\big(T_R(j) \leq t < T_R(j+1)\big) = T_R(j+1) - T_R(j),$$
$$RRI\big(t < T_R(1)\big) = RRI\big(t = T_R(1)\big),$$
$$RRI\big(t > T_R(J-1)\big) = RRI\big(t = T_R(J-1)\big),$$

$$(j = 1,2, \dots, J - 1)$$

where $T_R(j)$ represents the time for the j-th R-wave peak and the J represents total number of the detected R-wave peaks at the given trial. The estimated instantaneous RRI data were then smoothed with the Gaussian filter with 235 ms FWHM and z-transformed within each individual.

Similarly to the pupil data, the trial-by-trial summary for the SCL, SCR, and RRI data were defined as follows. The tonic SCL was defined as the average of SCL during the pre-movement period. The phasic SCR responses to perturbation were defined as the average values for the temporal ROIs detected by the cluster-based permutation test of the time series data for the small against the large perturbation for onset-aligned data (Table 1 and 3, Small vs. Large). We opted to choose the offset-aligned data for the phasic RRI responses (Table 2 and 4, Small vs. Large).

Statistical analyses

Timeseries comparison. To detect the significant effects of perturbation size (small vs. large) in the autonomic response time series data, we applied the cluster-based permutation test (Maris and Oostenveld, 2007). The overall alpha-level was set to $p < 0.05$, the cluster-forming threshold was set to $p < 0.01$, the test directionality was set to two-sided, and the permutation number was 10^4. We used the Matlab implementation of the test by E. Gerber (permutest.m; https://www.mathworks.com/matlabcentral/fileexchange/71737-permutest). As a complement, we also employed a mass t-test, a simple series of t-tests on each time frame, corrected for false-discovery rate ($q < 0.05$) (Benjamini and Hochberg, 1995). We use the Matlab implementation of the correction by D. Groppe (fdr_bh.m; https://www.mathworks.com/matlabcentral/fileexchange/27418-fdr_bh). For our experiments, the two tests yield similar results (Yokoi and Weiler, 2022).

SEM modeling. To assess the relationship between the phasic autonomic responses to errors and the single-trial learning rate, we applied the structural equation modeling (SEM). We defined a path diagram based on a hypothesis that the autonomic responses affect the learning rate (Fig. 6E). As manifest (observed) variables, we used the autonomic response summary data (delta-pupil dilation velocities, delta-SCR, and delta-zRRI), the error data, and the single-trial learning rate data, averaged within each perturbation size. As latent (construct) variables, we defined the sympathetic activity state ('*Sym*'), the parasympathetic activity state ('*Para*'), the prediction error (or could be called surprise) ('*PE*'), and the learning rate ('*LR*') (Fig. 6E). The '*PE*' was assumed to be formative, and the other latent variables were assumed to be reflective. The path diagram was defined based on the physiological evidence and SEM modeling requirements. We assumed that only '*Para*' affects RRI index as the kinetics of sympathetic drive on the heart rate is much slower compared to parasympathetic drive (Berger et al., 1989; Ng et al., 2001). Similarly, we also assumed that the SCR

index was directly affected only by '*Sym*', as the sweat grand is solely innervated by sympathetic terminals (Dawson et al., 2007). While pupil diameter is regulated by both sympathetic and parasympathetic pathways, we assumed that the pupil indices were directly affected by '*Sym*' only. The effect from parasympathetic pathway was expressed as a path from '*Para*' to '*Sym*'. Although this path also affects the SCR index, we decided to employ the current path diagram, as more complex diagrams with SCR and pupil indices separated yielded path coefficients inconsistent with known physiological evidence that pupil dilation/constriction is regulated by sympathetic/parasympathetic activity (Supplementary Material). As our latent variables contain one formative construct ('PE') and data is not normally distributed, we chose to apply partial least square SEM (PLS-SEM) approach (Vinzi et al., 2010). The opposite path from '*Sym*' to '*Para*', which makes the path diagram cyclic, was omitted to void loops in PLS-SEM modeling (Vinzi et al., 2010). We used the PLS-SEM Toolbox developed by M. Aria (https://www.mathworks.com/matlabcentral/fileexchange/54147-pls-sem-toolbox). The 95% confidence intervals for the factor loading and path coefficients were estimated through the bootstrapping. We conducted participant-wise resampling for 5000 times.

Data and code availability

The data and the custom-written Matlab codes used for the analysis will be uploaded to the publicly available server upon publication.

Results

To assess error-induced autonomic responses during motor learning, we simultaneously monitored the pupil diameter, SCL, and ECG, while human participants made reaching movement (Fig. 1A). To accurately evaluate motor learning, we employed the single-trial adaptation paradigm (Marko et al., 2012; Kasuga et al., 2013), where different sizes of error were applied unexpectedly to the participants, and the learning is assessed by comparing the movements between trials immediately before and after the error trial. The three consecutive trials (pre, perturbation, and post trials), called 'triplet', were followed by a sequence of normal trials with no perturbation (ranging from 4 to 6 trials length) and repeated. In Experiment 1 (n = 39), we manipulated proprioceptive errors, while in Experiment 2 (n = 39), we manipulated visual cursor errors, with the error direction and magnitude randomly selected from one of nine angles (±45°, ±30°, ±10°, ±5°, 0°). (Fig. 1B, C). The two experiments were conducted independently, and participants did not overlap between experiments.

Phasic autonomic responses to proprioceptive errors at distinct time windows (Exp 1)

We first evaluated the phasic change in autonomic signal during reaching task and their responses to movement errors. For the pupil diameter and the SCL data, we took time-derivative to separate them from the tonic activity and obtained pupil dilation velocity and skin conductance response (SCR). For the ECG data we evaluated the smoothed z-transformed R-R interval (RRI). Figure 2 shows the average time course of the pupil dilation velocity, SCR, and RRI for Exp 1, each aligned either to movement onset (left column), or offset (right column). As we did not provide any visual cursor nor endpoint feedback during the perturbation trials, the error modality was restricted to proprioception.

During the normal reaching trials ('Null'), pupil (dilation) velocity and RRI showed typical response observed in cue-response type tasks (van der Molen et al., 1989), whereas SCR showed minor change (Fig. 2). When we introduced proprioceptive error by mechanically constraining the reach trajectory (Fig. 1B), these autonomic indices exhibited clear phasic response to the errors with specific latencies and the size of response was error size-dependent (Fig. 2). To distill the error-induced response components from the autonomic response time series, we first defined the temporal regions of interest (ROIs) by comparison between the small error (0°, ±5°, ±10°) trials ('Small') vs. large error (±30°, ±45°) trials ('Large'). The averaged response data for the ROIs were later assessed in detail and further submitted to path analyses to test the potential effect of autonomic responses to learning rate.

The comparison between the Small and the Large conditions revealed three separate temporal ROIs for the pupil dilation velocity, with two dilation components followed by a constriction component (Fig. 2A; Table 1). The first error-induced dilation started during movement as early as 170 msec since movement onset (Fig. 2A) and this was clearly due to proprioceptive error during movement. The other two ROIs were located after the movement termination (Fig. 2A, B). For the SCR, the same comparison between 'Small' vs. 'Large' conditions revealed clear increase in SCR

dependent on error size at around 1595 msec since movement onset (Fig. 2C). Considering the slow latency of SCR (typically 1.0 ~ 3.0 sec from an event), this SCR is attributed to the proprioceptive error experienced during movement. It is thus likely that the initial error-induced pupil response was driven by sympathetic upregulation rather than parasympathetic withdrawal, since sweat gland is predominantly innervated by sympathetic fibers (Dawson et al., 2007). Such sympathetic drive during movement was, however, not visible in the RRI, presumably due to the slower kinetics of sympathetic nerve effects on heart rate (Berger et al., 1989; Ng et al., 2001). Instead, the RRI responded to proprioceptive error in more parasympathetic direction (Fig. 2E, F). This RRI increase (i.e., heart rate deceleration) started after movement offset and showed more pronounced statistical effect when aligned to movement offset (Fig. 2F, Table 2), suggesting the possible connection with post-movement evaluation/reflection process. Previous study also reported the RRI increase after error commission in the choice reaction task (Danev and de Winter, 1971). In sum, the autonomic measures we collected (pupil dilation velocity, SCR, and RRI) showed clear responses to unexpected proprioceptive errors, and their magnitude could reflect both in-movement and post-movement processes, such as sensory surprise and/or orienting response during movement and post-movement outcome evaluation/reflection. Next, to look more closely into the error size-dependency of these autonomic responses, we analyzed the difference in these responses between pre and perturbation trials, for each error direction, size, and time window (Fig. 3).

Error size-dependent modulation of phasic autonomic responses to proprioceptive errors (Exp 1)

As shown in Figure 3, trial summary values of the phasic autonomic responses in each temporal ROI increased as a function of error size, indexed by the amount of force impulse received during the perturbation trials. The magnitude of proprioceptive errors was lager for the rightward perturbations (defined as positive in Fig. 3), possibly because of the biomechanical property (e.g., stiffness) of the right arm (Gomi and Kawato, 1996, 1997). Interestingly, a visual inspection indicated that such asymmetry in the proprioceptive error for the same categorical perturbation sizes (e.g., +45° vs -45°) looked well-explaining the size differences in phasic autonomic responses (Fig. 3). Thus, the phasic autonomic responses seem sensitive to the discrepancy between expected and actual force to the hand in a dose dependent manner. As the error-induced pupil dilation diminishes during the step-like force-field perturbation schedule, despite participants' learning to compensate for the force (Yokoi and Weiler, 2022), it is more likely that these phasic autonomic responses in the current study were driven by prediction error, rather than by physical effort. In summary, the current results demonstrated that the phasic pupil dilations followed by a constriction, SCR, and post-movement heart-rate deceleration tracks the size of proprioceptive error during movement. We next sought to test whether this is also the case for the visual errors (Exp 2).

Phasic autonomic responses to visual errors (Exp 2)

We conducted the variant of the Exp 1 where the visual errors were applied by rotating the cursor trajectory (i.e., visuomotor rotation) with a new set of participants (Fig. 1C). Thus, in contrast to the Exp 1, we provided continuous visual cursor feedback in this Exp 2, except for the post-perturbation trials where learning was probed in no feedback condition. This is to make the two experiments comparable by making online error information during reaching movements available. We also did not provide the endpoint feedback during the perturbation trial for the same comparability purpose.

When no perturbation was applied ('Null'), pupil (dilation) velocity, SCR, and RRI showed similar response time course to that for Exp 1 (Figs. 2 and 4). For the error response, however, although qualitatively similar, the visuomotor perturbations elicited only weak responses for the pupil and SCR (Fig. 4A-D). The first temporal ROI for significant error size effect ('Small' vs. 'Large') in pupil dilation shifted in time (170 msec vs. 405 msec; Fig. 4A; Table 3). When we compare the range of the phasic response for the pupil and SCR in the first ROI across the experiments, the response range for Exp 2 roughly matched to that of Exp 1 for 'Small' perturbation (Figs. 3 and 5). Regarding pupil responses for other ROIs and RRI, the response range was comparable across the experiments (Fig. 4). Overall, although the magnitude of error response was weak in some measures in Exp 2, autonomic measures showed qualitatively similar response in terms of error size-dependency across the experiments.

Possible association between phasic autonomic error responses and single-trial learning rate

So far, we observed that the magnitude of phasic autonomic responses increased as the size of induced movement error increased. Such increase in autonomic tone could either directly or indirectly affect motor learning process. For instance, as reported in previous studies, the learning rate (sensitivity to errors) typically decreases for large errors compared to the small errors (Fine and Thoroughman, 2006; Wei and Körding, 2009; Marko et al., 2012; Kasuga et al., 2013; Hayashi et al., 2020). Similarly, awareness to the perturbation depends on perturbation size (Werner et al., 2015) and reportedly suppresses the implicit motor learning (Kagerer et al., 1997; Sakaguchi et al., 2001; Benson et al., 2011; Neville and Cressman, 2018). Consistently, such pattern was also present in our data (Fig. 6A-D). Across-trial corrections for larger errors were relatively smaller compared to those for smaller errors (Fig. 6A, C), and sensitivity to error decreased as the error size increased (Fig. 6B, D). Based on these observations, we hypothesized that the error-induced phasic autonomic activity could mediate the error size-dependent modulation of single-trial learning rate.

To test the hypothesis, we evaluated the effect of phasic autonomic error responses on motor learning rate by using the structural equation modeling (SEM) and fitted the hypothetical relationship between observed and latent variables in the current study (Fig. 6E). Here, we assumed three reflective

latent states to express the fluctuation of the sympathetic ('Sym') and the parasympathetic ('Para') activities, as well as the learning rate ('LR') and one formative latent state for internal representation of unsigned prediction error ('PE'), for each perturbation condition for each individual (Fig. 6E, see Methods for more detail). In this setting, the significant positive/negative path from the autonomic state (Sym/Para) to the LR together with the significant path from PE to Sym/Para indicate statistical mediation of learning rate modulation by autonomic state.

The path model shown in the Figure 6E yielded a good fit; the standardized root mean square residual (SRMR) was less than 0.08 (=0.0559) and the Tucker and Lewis index (TLI) was higher than 0.95 (=0.9668). The confirmatory factor analysis using SEM applied onto the Exp 1 data revealed significant positive paths from the 'PE' to both the 'Para' and 'Sym' (the bootstrapped 95% confidence interval was [0.084, 0.282] and [0.691, 0.808], respectively), consistent with previous studies suggesting that a surprising event drives both of sympathetic and parasympathetic activities (Danev and de Winter, 1971; Murphy et al., 2016; Roelofs and Dayan, 2022). The analysis also revealed a significant negative path from the 'Para' to the 'Sym' (the bootstrapped 95% confidence interval: [-0.539, -0.345]), reflecting the opposite relationship between the parasympathetic and sympathetic system. Remarkably, the analysis revealed a significant negative path from the 'Sym' to the 'LR' (the bootstrapped 95% confidence interval: [-0.268, -0.043]), while it was not the case for the path from the 'Para' to the 'LR' (the bootstrapped 95% confidence interval: [-0.13, 0.036]). Additionally, although the overall effect direction was negative, the path from the 'PE' to the 'LR' did not reach significance (the bootstrapped 95% confidence interval: [-0.13, 0.033]), indicating the full-mediation effect of error-induced sympathetic activity in the error size-dependent modulation of learning rate.

Contrary to the result for the Exp 1, the same structure model applied to the Exp 2 data yielded slightly different results, while the fit was decent (SRMR = 0.0539, TLI = 1.0196). Although the significance and the direction of effects for paths between 'PE' and 'Sym' (the bootstrapped 95% confidence interval: [0.401, 0.581]), 'PE' and 'Para' (the bootstrapped 95% confidence interval: [0.004, 0.276]), and 'Para' and 'Sym' (the bootstrapped 95% confidence interval: [-0.607, -0.434]) were consistent with the Exp 1, the path from 'Sym' to 'LR' was not significant (the bootstrapped 95% confidence interval: [-0.138, 0.086]). Instead, the model estimated the significantly positive path from 'Para' to 'LR' (the bootstrapped 95% confidence interval: [0.032, 0.189]). The overall effect direction from the 'PE' to the 'LR' was, again, negative, but did not reach significance (the bootstrapped 95% confidence interval: [-0.304, 0.041]).

Taken together, although there was a mismatch between the two experiments, our results suggest the possible involvement of error-induced autonomic states in the modification of trial-by-trial motor learning rate. The discrepancy between the experiments may be attributed to the substantial difference in the amount of phasic autonomic responses to errors between the experiments.

Discussion

In this study, we investigated changes in pupil diameter, skin conductance, and heart rate in response to motor errors during reaching movement to characterize how autonomic nervous system (ANS) respond during single-trial motor adaptation with either proprioceptive (Exp 1) or visual (Exp 2) errors. The results demonstrated that all three ANS indices exhibited qualitatively similar responses to errors across the experiments, while the magnitude was much higher in Exp 1. Each ANS index we measured responded to motor errors in specific time windows and their response sizes were scaled by error size. Furthermore, our data suggest that the autonomic states may mediate the error size-dependent adjustment of motor learning rate, although the detail of the mediation effect was different across the experiment.

The discrepancy between the results for Exp 1 and 2

While the ANS responses to motor errors were qualitatively similar across the error modalities, the magnitude showed marked difference, with response to proprioceptive error (Exp 1) much greater and earlier than that to visual error (Exp 2). The difference was the most pronounced for the first peak in the pupil dilation and SCR, while the other pupil response peaks and RRI change was relatively similar across the experiment. One possible reason is that visual errors might have been perceived less prominent than proprioceptive errors due to the current experimental setting. In the current study, participants were required to fixate on the target which was located at 10 cm away from the starting position which was approximately 13º eccentricity in visual angle in the current setting. This may have caused errors to fall outside the foveal view. Considering the lower spatial acuity in peripheral vision (Carrasco et al., 1995; Carrasco and Barbot, 2014), the detection of visual error might have been insufficient or delayed significantly which resulted in weaker change in internal states, such as surprise, in the Exp 2. This explains that the first phasic pupil error response peak was weak and delayed in time (Fig. 4A). Also consistent with this is that the estimated learning rates for the Exp 2 in the current study (Fig. 6D) were relatively small compared to the values estimated in the similar experiment without strict fixation requirement (Figure 2B in Kasuga et al., 2013). The additional possibility is that visual errors activated the LC neurons less directly than proprioceptive errors did. LC neurons receive direct spinal projections (Szabadi, 2013; Poe et al., 2020), while visual error, except for luminance input, reaches to LC more indirectly, through superior colliculus (Wang and Munoz, 2015; Joshi and Gold, 2020) and/or cortical regions (Corneil and Munoz, 2014). Therefore, from the quantitative perspective, it may not be easy to directly compare the Exp 1 and 2 with respect to the error modality, as well as to the potential influence of ANS activity on motor learning rate. For this reason, we restrict our discussion provided below mainly to the Exp 1 results.

Possible influence of phasic autonomic activity on motor learning rate

The negative path between the latent sympathetic state and the latent learning rate state identified by the SEM analysis suggests that the excess amount of sympathetic (LC-NA) activity for large errors reduces the sensitivity to errors. There are several possible scenarios that could explain the above relationship in parallel. Perhaps the most direct pathway would be the projection from the LC to the cerebellum (Bloom et al., 1971; Olson and Fuxe, 1971; Szabadi, 2013). Several studies demonstrated that the NA reduces the probability of complex spike in cerebellar Purkinje cells, a key element for error-based motor learning, through the alpha2-adrenergic receptor (Carey and Regehr, 2009; Sun et al., 2019). It has also been suggested that in the cerebellum, the alpha2-adrenergic receptor is dominant in high NA concentration, while the beta-adrenergic receptor is dominant in low NA concentration (Wakita et al., 2017). This scenario does not necessary require the involvement of conscious awareness and explicit cognitive processes. Another possibility is that the error-driven phasic autonomic (LC-NA) responses only reflect the increased participation of explicit cognitive processes in motor learning and do not directly modify learning rate. In turn, the explicit cognitive processes suppress the (implicit) motor learning (Kagerer et al., 1997; Sakaguchi et al., 2001; Benson et al., 2011; Neville and Cressman, 2018) via some unknown mechanism, such as divided (Taylor and Thoroughman, 2007, 2008) or impaired (Arnsten, 2009) attention to the task. Consistently, in a choice task requiring the cognitive control, the size of error-evoked pupil dilation predicted the degree of post-error slowing and behavioral adjustment in the following trial (Murphy et al., 2016). In sum, either one or both above hypothetical pathways could be responsible for the observed effect of phasic autonomic responses to reduction in the learning rate. These mechanisms could be the effective implementation of the normative Bayesian interpretation of the 'relevance of error' (Wei and Körding, 2009).

It should be noted, however, that we still observed the error size-dependent reduction in the learning rate in Exp 2 despite the weak autonomic responses to errors. Therefore, there may be certainly more mechanisms for adjusting motor learning rate than raised above. One, such mechanism is the divisive normalization of error itself, rather than sensitivity to it (Hayashi et al., 2020; Makino et al., 2023). Another more relevant explanation is increased visual uncertainty for large visual perturbations (Zhang et al., 2024).

The time course of autonomic responses to motor errors and underlying cognitive processes

The current results captured temporally dynamic nature of ANS responses induced by unexpected errors during motor learning task. These responses initiated primarily from the sympathetic upregulation as reflected by increased pupil dilation and SCR and then was followed by parasympathetic dominance as reflected by heart rate deceleration. This is also consistent with the significant positive paths from prediction error state to both the sympathetic and parasympathetic states revealed in the current latent factor analysis. We expect that these ANS responses could reflect

multiple cognitive processes triggered by motor errors some of which may also be related with LC-NA activity.

The initial error-evoked pupil dilation starting as early as ~200 msec after movement onset may reflect the orienting response to unexpected sensory event (Sara and Bouret, 2012). The orienting response has also been associated with event-related potential (ERP) of electro-encephalography (EEG), especially the P300 or P3b, and is also considered LC-NA dependent (Polich, 2007; Murphy et al., 2011). Importantly, this ERP component has long been considered to reflect the updating of context (i.e., internal model of external world) mediated by prefrontal cortex (Donchin and Coles, 1988; Polich, 2007; Lenartowicz et al., 2010), which is also fundamental for motor learning (Heald et al., 2023). In fact, the LC-NA activity in orienting response has also been found to be critical for context-dependent memory retrieval in animals (Sara and Bouret, 2012). The other post-movement error-induced pupil responses and RRI increase may also be associated with the similar orienting and/or context updating processes. Alternatively, they could also be associated with feedback-related ERP component, such as feedback related negativity, which is suggested to reflect reward-based learning (Walsh and Anderson, 2012; Palidis et al., 2019; Palidis and Gribble, 2020).

The observed sequence of sympathetic and parasympathetic activation bears some resemblance to the similar ANS responses during fear response, such as "freezing" (Roelofs and Dayan, 2022). Recent works proposed that the freezing is more active state than previously thought with boosted sensory and cognitive processing to analyze situation and prepare to act (Roelofs and Dayan, 2022). Thus, although we need further studies, the expression of cognitive processes, such as aiming or strategy use (McDougle et al., 2015; Tsay et al., 2024) triggered by large, responses to unexpected movement errors may also share similar mechanism with more innate response to threat, such as contextual learning. Taken together, autonomic indices could provide valuable insights into multiple cognitive processes during motor learning.

Limitation

Although our experimental design has a form that manipulated the ANS activity by applying motor errors with different magnitude, more direct manipulation technique is required in order to causally test the involvement of ANS (or LC-NA system) in the adjustment of motor learning rate. Future invasive animal study or non-invasive stimulation of LC would extend our finding. These apporaches are necessary to test the contribution of ANS (LC-NA system) fluctuation in motor learning rate, while keeping the amount of error and possible normalization effect (Hayashi et al., 2020; Makino et al., 2023) constant. Another limitation of the curent study is that we did not explicitly measured participants' awareness about the perturbation and nor assesed the explicit learning measures, such as re-aiming strategy. Thus, although we expect the participation of explicit cognitive process triggered by the awareness in large motor error conditions (Fernandez-Ruiz et al., 2011; Haith et al., 2015;

Huberdeau et al., 2015) and it could have suppressed the implicit learning (Kagerer et al., 1997; Sakaguchi et al., 2001; Benson et al., 2011; Neville and Cressman, 2018), it is only circumstantial and remains speculative. Further studies that simultaneously assess the error awareness, explicit learning component, and autonomic measures will clarify this issue.

Conclusion

The current study systematically characterized the changes in pupil diameter, SCR, and RRI in response to sudden errors during motor adaptation. We suggest that autonomic nervous system responses during motor learning may reflect dynamic changes in internal states triggered by unexpected errors. Closer look at autonomic activity may help us better understand the cognitive processes and physiological mechanisms underlying motor learning.

Acknowledgements

This work was supported by JSPS KAKENHI (JP22H03501 and JP23K24758) and JST FOREST program (JPMJFR234Z) awarded to AY. M.N. is supported by a fellowship from JST SPRING program (JPMJSP2138). We thank Saeko Kato for assistance in data collection.

Conflict of interest

None declared.

Author contributions

A.Y. conceived and designed research; A.Y. and M.N. performed experiments; A.Y. and M.N. analyzed data; A.Y. and M.N. interpreted results of experiments; A.Y. and M.N. prepared figures and tables; M.N. drafted manuscript; A.Y., M.N. and N.H. edited and revised manuscript; A.Y., M.N. and N.H. approved final version of manuscript.

Figures

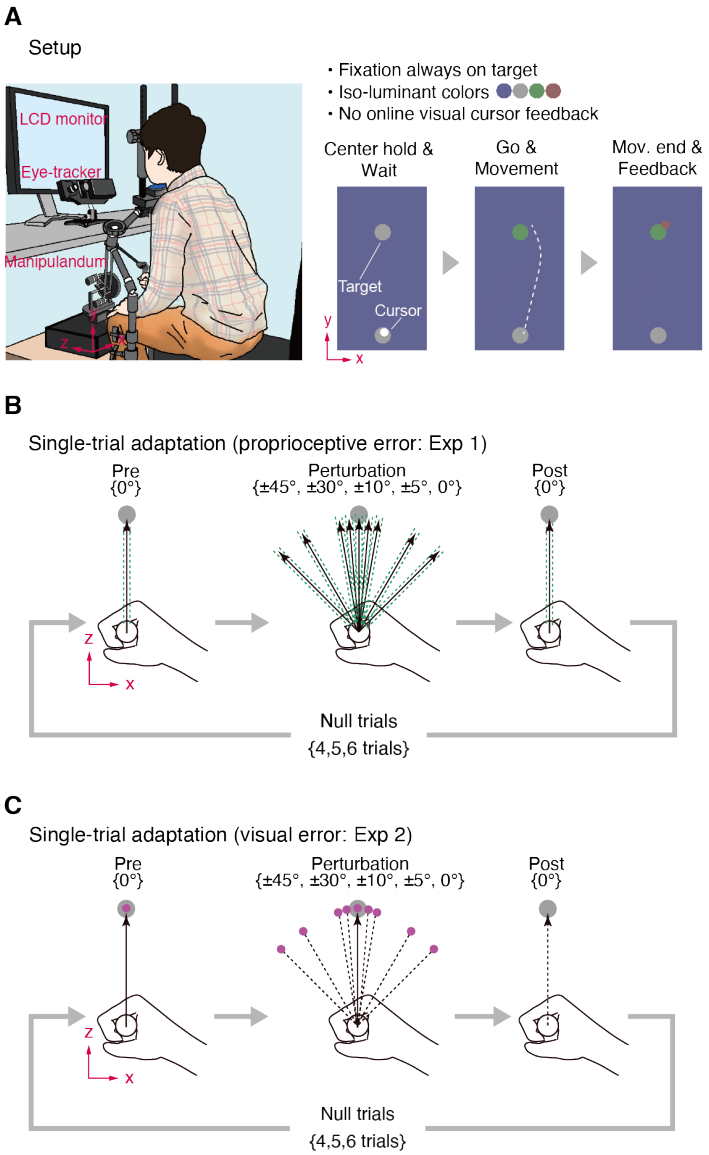

Figure 1. Simultaneous acquisition of multimodal autonomic signals (pupil, skin conductance, and heart rate) during single-trial motor adaptation paradigm.

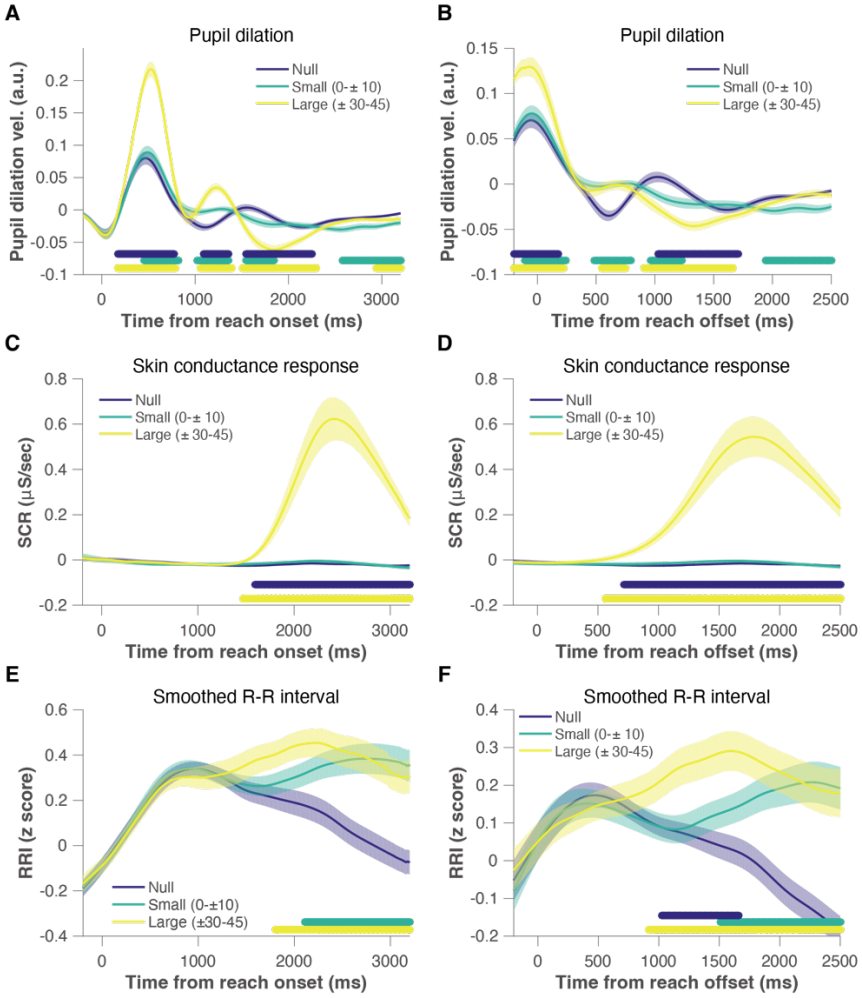

Figure 2. Time profiles of phasic autonomic responses to proprioceptive errors (Exp 1).

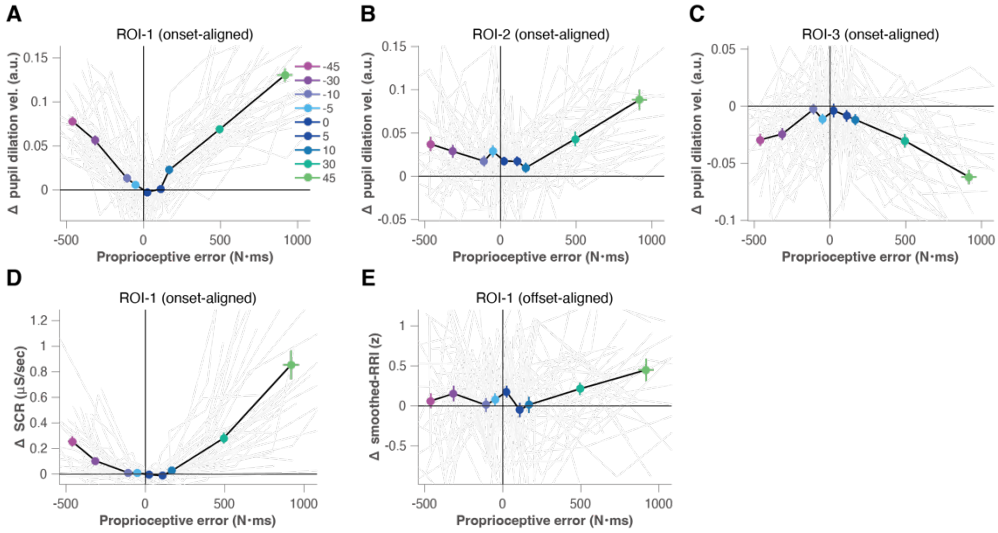

Figure 3. Mean phasic autonomic responses as a function of proprioceptive error magnitude.

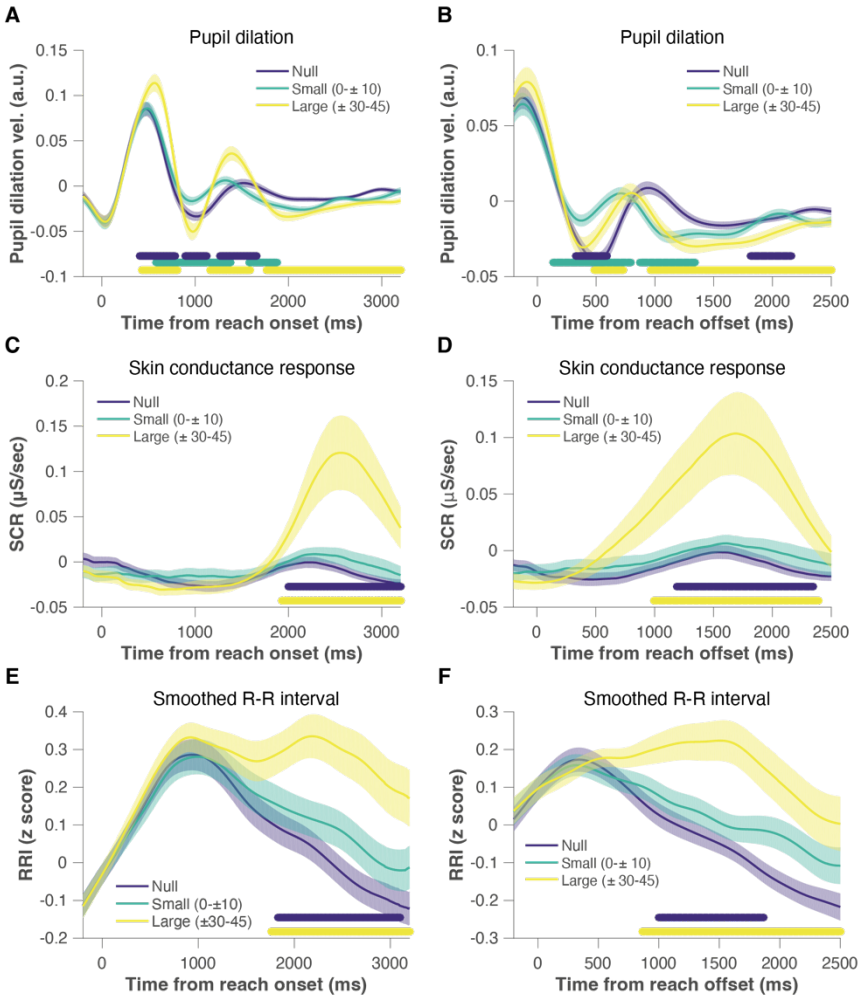

Figure 4. Time profiles of phasic autonomic responses to visual errors (Exp 2).

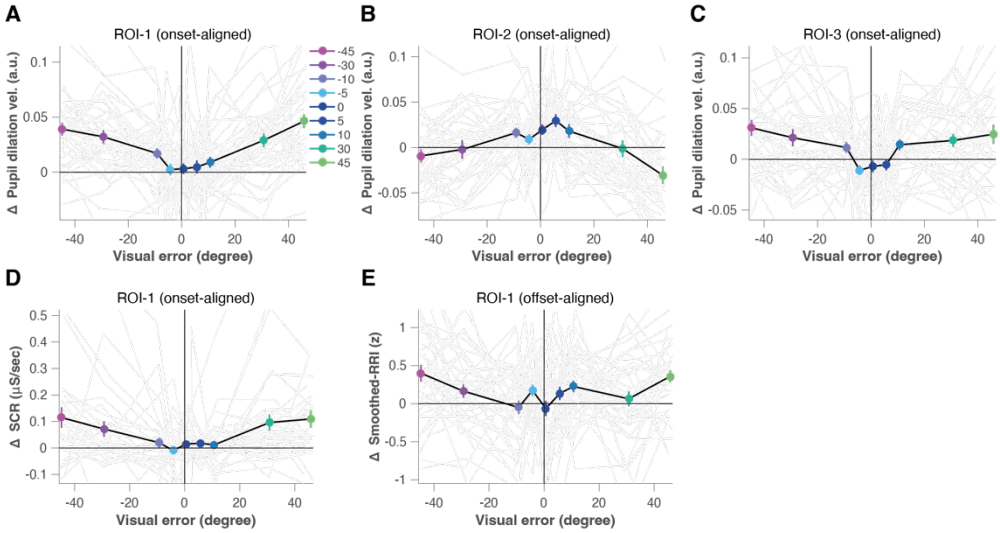

Figure 5. Mean phasic autonomic responses as a function of visual error magnitude.

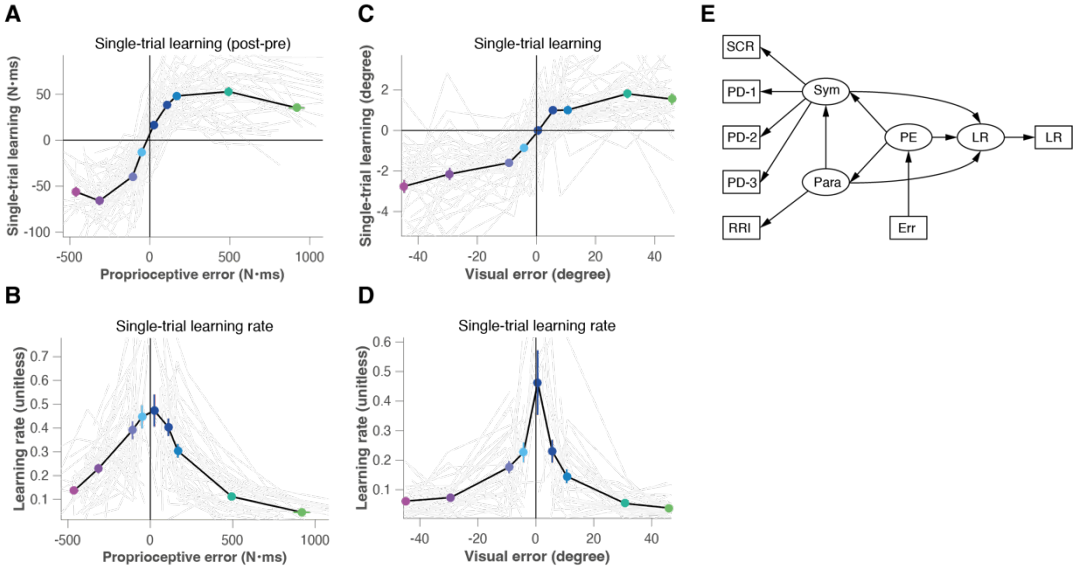

Figure 6. Single-trial motor learning and latent autonomic states.

Figure legends

Figure 1. Simultaneous acquisition of multimodal autonomic signals (pupil, skin conductance, and heart rate) during single-trial motor adaptation paradigm. (A) Experimental set up for experiment 1 and 2. We measured pupil diameter, skin conductance, and electrocardiogram of participants while they performed reaching movement holding a handle of robotic manipulandum. (left). Participants initially practiced making straight reaching movements to hit a cursor into a target (right). In the main session, however, the online cursor feedback was occluded, and only terminal feedback was provided. **(B, C)** Single-trial adaptation to various sizes of error was assessed by comparing the movements in trials immediately before ('Pre') and after ('Post') the perturbation trial. In the Exp 1, we assessed the adaptation to proprioceptive error by constraining the reach trajectory in 9 different directions with a simulated 'force channel' (B). In pre- and pot-perturbation trials, we measure the participants' force in the perpendicular direction to the movement with the force channel. No endpoint feedback was provided in the perturbation trials to minimize the mismatch between visual and proprioceptive information. In the Exp 2, we assessed the adaptation to visual error by applying the visuomotor rotation of the cursor in 9 possible angles. To this end, continuous visual cursor feedback was provided. No feedback was provided in the post-perturbation trials.

Figure 2. Time profiles of phasic autonomic responses to proprioceptive errors (Exp 1). (A, C, E) Phasic error responses measured at perturbation trials for pupil dilation velocity (A), skin conductance response (C), and smoothed R-R interval (E) data aligned to the timing of movement onset. **(B, D, F)** Phasic error responses for pupil dilation velocity (B), skin conductance response (D), and R-R interval (F) data aligned to the timing of movement offset. Shaded area represents the standard error of the mean (SE). Null: Normal reach trials interspersed between the 'triplet' trials (Fig. 1B). Small: Perturbation trials with small proprioceptive errors (between -10º and 10º). Large: Perturbation trials with large proprioceptive errors (±30º, ±45º). The sequence of colored dots below the traces indicate the significant (p<0.05) clusters assessed by the cluster permutation test (Maris and Oostenveld, 2007). Blue: Comparison between Small vs. Large. Green: Small vs. Null. Yellow: Large vs. Null. The detailed statistics are presented in the Tables 1 (onset-aligned data) and 2 (offset-aligned data).

Figure 3. Mean phasic autonomic responses as a function of proprioceptive error magnitude. The temporal regions of interest (ROIs) were defined by the significant clusters shown in Fig. 2. Mean phasic autonomic signal data within each ROI were compared between perturbation vs. pre-perturbation trials to yield delta-response data. **(A-C)** The mean delta-pupil dilation velocity for the ROI-1 (A), ROI-2 (B), and ROI-3 (C), respectively (Fig. 2A). **(D)** The mean delta-SCR for the ROI-

1 (Fig. 2C). (E) The mean delta-smoothed-RRI for the ROI-1 (Fig. 2F). Error-bars indicate the SEs for each of x-y values within each perturbation condition. Thin grey lines represent individual data.

Figure 4. Time profiles of phasic autonomic responses to visual errors (Exp 2). (A, C, E) Phasic error responses measured at perturbation trials for pupil dilation velocity (A), skin conductance response (C), and smoothed R-R interval (E) data aligned to the timing of movement onset. **(B, D, F)** Phasic error responses for pupil dilation velocity (B), skin conductance response (D), and R-R interval (F) data aligned to the timing of movement offset. Shaded area represents the standard error of the mean (SE). Null: Normal reach trials interspersed between the 'triplet' trials (Fig. 1B). Small: Perturbation trials with small proprioceptive errors (between -10º and 10º). Large: Perturbation trials with large proprioceptive errors (±30º, ±45º). The sequence of colored dots below the traces indicate the significant (p<0.05) clusters assessed by the cluster permutation test (Maris and Oostenveld, 2007). Blue: Comparison between Small vs. Large. Green: Small vs. Null. Yellow: Large vs. Null. The detailed statistics are presented in the Tables 3 (onset-aligned data) and 4 (offset-aligned data).

Figure 5. Mean phasic autonomic responses as a function of visual error magnitude. The temporal regions of interest (ROIs) were defined by the significant clusters shown in Fig. 4. Mean phasic autonomic signal data within each ROI were compared between perturbation vs. pre-perturbation trials to yield delta-response data. **(A-C)** The mean delta-pupil dilation velocity for the ROI-1 (A), ROI-2 (B), and ROI-3 (C), respectively (Fig. 4A). **(D)** The mean delta-SCR for the ROI-1 (Fig. 4C). (E) The mean delta-smoothed-RRI for the ROI-1 (Fig. 4F). Error-bars indicate the SEs for each of x-y values within each perturbation condition. Thin grey lines represent individual data.

Figure 6. Single-trial motor learning and latent autonomic states. (A, C) Single-trial learning (across-trial correction) as a function of proprioceptive (A) or visual (C) error size. Linear increase in correction only holds for small errors. **(B, D)** Single-trial learning rate as a function of proprioceptive (B) or visual (D) error size. **(E)** A path-diagram for hypothetical relationship across the observed (rectangles) and latent (ellipses) variables. SCR: The averaged SCR for each perturbation condition (Fig. 3D or Fig. 5D). PD-1~3: The averaged pupil dilation velocity for the ROI-1~3 for each perturbation condition (Fig. 3A-C or Fig. 5A-C). RRI: The averaged smoothed RRI for each perturbation condition (Fig. 3E or Fig. 5E). Sym: The latent state for sympathetic activity. Para: The latent state for parasympathetic activity. PE: The latent state for surprise (unsigned prediction error). LR: The latent state for learning rate. Error-bars indicate the SEs for each of x-y values within each perturbation condition. Thin grey lines represent individual data. The estimates and the bootstrapped 95% CIs for the path coefficients and loadings are presented in Tables 5 (path coefficients) and 6 (loadings).

Tables

Table 1. Temporal ROIs for significant effect of proprioceptive perturbation (Exp 1) tested over the phasic autonomic response time series aligned to movement onset (Fig. 2, left column).

Variables	Comparison	Start	Center	End	Extent	p-Values
Pupil velocity	Null vs Large	170	480	790	620	1.00×10^{-4}
		1510	1900	2295	785	1.00×10^{-4}
		2940	3235	3535	595	0.002
		1060	1225	1395	335	0.002
	Null vs Small	2575	3050	3525	950	1.00×10^{-4}
		455	635	820	365	0.003
		1025	1190	1360	335	0.004
		1545	1695	1845	300	0.022
	Small vs Large	170	470	775	605	1.00×10^{-4}
		1545	1900	2255	710	1.00×10^{-4}
		1090	1225	1360	270	0.014
SCR	Null vs Large	1465	2455	3445	1980	1.00×10^{-4}
	Small vs Large	1595	2545	3495	1900	1.00×10^{-4}
RRI	Null vs Large	1800	2705	3610	1810	1.00×10^{-4}
	Null vs Small	2110	2775	3440	1330	1.00×10^{-4}

We used cluster-based permutation test (Maris and Oostenveld, 2007). The overall alpha-level was set to $p < 0.05$, the cluster-forming threshold was set to $p < 0.01$, the test directionality was set to two-sided, and the permutation number was 10^4. Units are in msec. Data within each comparison type are ordered according to p-values.

Table 2. Temporal ROIs for significant effect of proprioceptive perturbation (Exp 1) tested over the phasic autonomic response time series aligned to movement off (Fig. 2, right column).

Variables	Comparison	Start	Center	End	Extent	p-Values
Pupil velocity	Null vs Large	910	1285	1665	755	1.00×10^{-4}
		-200	10	225	425	0.0003
		2515	2755	2995	480	0.002
		545	650	755	210	0.034
	Null vs Small	1940	2465	2995	1055	1.00×10^{-4}
		485	640	795	310	0.001
		-105	70	245	350	0.002
		965	1100	1235	270	0.030
	Small vs Large	1025	1365	1710	685	0.0002
		-200	-10	180	380	0.0002
SCR	Null vs Large	560	1700	2845	2285	1.00×10^{-4}
	Small vs Large	715	1800	2885	2170	1.00×10^{-4}
RRI	Null vs Large	915	1870	2830	1915	1.00×10^{-4}
	Null vs Small	1505	2165	2830	1325	0.0003
	Small vs Large	1020	1340	1665	645	0.028

We used cluster-based permutation test (Maris and Oostenveld, 2007). The overall alpha-level was set to $p < 0.05$, the cluster-forming threshold was set to $p < 0.01$, the test directionality was set to two-sided, and the permutation number was 10^4. Units are in msec. Data within each comparison type are ordered according to p-values.

Table 3. Temporal ROIs for significant effect of visual perturbation (Exp 2) tested over the phasic autonomic response time series aligned to movement onset (Fig. 4, left column).

Variables	Comparison	Start	Center	End	Extent	p-Values
Pupil velocity	Null vs. Large	1765	2535	3310	1545	1.00×10^{-4}
		425	620	815	390	6.00×10^{-4}
		1155	1370	1590	435	2.00×10^{-3}
	Null vs. Small	580	980	1385	805	1.00×10^{-4}
		1575	1725	1875	300	3.06×10^{-2}
	Small vs. Large	405	595	785	380	1.00×10^{-4}
		1265	1465	1665	400	1.70×10^{-3}
		890	1005	1125	235	3.13×10^{-2}
SCR	Null vs. Large	1930	2630	3330	1400	6.00×10^{-4}
		-930	-645	-360	570	3.93×10^{-2}
	Null vs. Small	-725	-470	-210	515	4.76×10^{-2}
	Small vs. Large	2000	2610	3220	1220	1.00×10^{-3}
RRI	Null vs. Large	1755	2630	3510	1755	7.00×10^{-4}
	Small vs. Large	1830	2465	3105	1275	1.59×10^{-2}

We used cluster-based permutation test (Maris and Oostenveld, 2007). The overall alpha-level was set to $p < 0.05$, the cluster-forming threshold was set to $p < 0.01$, the test directionality was set to two-sided, and the permutation number was 10^4. Units are in msec. Data within each comparison type are ordered according to p-values.

Table 4. Temporal ROIs for significant effect of visual perturbation (Exp 2) tested over the phasic autonomic response time series aligned to movement offset (Fig. 4, right column).

Variables	Comparison	Start	Center	End	Extent	p-Values
Pupil velocity	Null vs. Large	960	1730	2500	1540	1.00×10^{-4}
		485	605	730	245	4.57×10^{-2}
	Null vs. Small	135	465	795	660	1.00×10^{-4}
		875	1110	1345	470	1.00×10^{-4}
	Small vs. Large	1815	1985	2160	345	9.00×10^{-3}
		325	455	590	265	2.94×10^{-2}
SCR	Null vs. Large	995	1690	2390	1395	1.00×10^{-4}
	Small vs. Large	1190	1770	2350	1160	9.00×10^{-4}
RRI	Null vs. Large	860	1845	2830	1970	5.00×10^{-4}
	Small vs. Large	1000	1435	1870	870	1.55×10^{-2}

We used cluster-based permutation test (Maris and Oostenveld, 2007). The overall alpha-level was set to $p < 0.05$, the cluster-forming threshold was set to $p < 0.01$, the test directionality was set to two-sided, and the permutation number was 10^4. Units are in msec. Data within each comparison type are ordered according to p-values.

Table 5. SEM results (path coefficients).

Experiments	Paths	Sample estimates	Bootstrapped 95% CIs
Exp 1	PE to Para	0.186	[0.084, 0.282]
	PE to Sym	0.753	[0.691, 0.808]
	PE to LR	-0.052	[-0.13, 0.033]
	Para to Sym	-0.441	[-0.539, -0.345]
	Para to LR	-0.047	[-0.13, 0.036]
	Sym to LR	-0.156	[-0.268, -0.043]
Exp 2	PE to Para	0.139	[0.004, 0.276]
	PE to Sym	0.494	[0.401, 0.581]
	PE to LR	-0.133	[-0.304, 0.041]
	Para to Sym	-0.518	[-0.607, -0.434]
	Para to LR	0.11	[0.032, 0.186]
	Sym to LR	-0.034	[-0.138, 0.086]

All values are standardized.

Table 6. SEM results (loadings).

Experiments	Variables	Sample estimates	Bootstrapped 95% CIs
Exp 1	PD-1	0.832	[0.784, 0.873]
	PD-2	0.63	[0.526, 0.727]
	PD-3	-0.681	[-0.767, -0.575]
	SCR	0.844	[0.795, 0.883]
Exp 2	PD-1	0.817	[0.68, 0.904]
	PD-2	-0.245	[-0.666, 0.3]
	PD-3	0.561	[0.273, 0.763]
	SCR	0.692	[0.423, 0.862]

Estimates for the manifest variables (Err, LR, and RRI) connected to the single-item constructs (PE, LR, and Para) were fixed to 1. All values are standardized.

References

‘t Hart BM, Taqvi U, Gastrock RQ, Ruttle JE, Modchalingam S, Henriques DYP (2024) Measures of Implicit and Explicit Adaptation Do Not Linearly Add. eNeuro 11:1–16.

Ahern S, Beatty J (1979) Pupillary responses during information processing vary with scholastic aptitude test scores. Science (80-) 205:1289–1292.

Albert ST, Jang J, Modchalingam S, ’T Hart M, Henriques D, Lerner G, Della-Maggiore V, Haith AM, Krakauer JW, Shadmehr R (2022) Competition between parallel sensorimotor learning systems. Elife 11:1–81.

Arnsten AFT (2009) Stress signalling pathways that impair prefrontal cortex structure and function. Nat Rev Neurosci 10:410–422.

Arnsten AFT, Wang MJ, Paspalas CD (2012) Neuromodulation of Thought: Flexibilities and Vulnerabilities in Prefrontal Cortical Network Synapses. Neuron 76:223–239 Available at: http://dx.doi.org/10.1016/j.neuron.2012.08.038.

Aston-Jones G, Cohen JD (2005) An integrative theory of locus coeruleus-norepinephrine function: Adaptive gain and optimal performance. Annu Rev Neurosci 28:403–450.

Aston-Jones G, Rajkowski J, Cohen J (2000) Locus coeruleus and regulation of behavioral flexibility and attention. Prog Brain Res 126:165–182.

Aston-Jones G, Rajkowski J, Kubiak P (1997) Conditioned responses of monkey locus coeruleus neurons anticipate acquisition of discriminative behavior in a vigilance task. Neuroscience 80:697–715 Available at: http://www.ncbi.nlm.nih.gov/pubmed/9276487.

Aston-Jones G, Rajkowski J, Kubiak P, Alexinsky T (1994) Locus coeruleus neurons in monkey are selectively activated by attended cues in a vigilance task. J Neurosci 14:4467–4480.

Benjamini Y, Hochberg Y (1995) Controlling the False Discovery Rate: A Practical and Powerful Approach to Multiple Testing. J R Stat Soc Ser B 57:289–300 Available at: http://www.jstor.org/stable/2346101.

Benson BL, Anguera JA, Seidler RD (2011) A spatial explicit strategy reduces error but interferes with sensorimotor adaptation. J Neurophysiol 105:2843–2851.

Berger RD, Saul JP, Cohen RJ (1989) Transfer function analysis of autonomic regulation. I. Canine atrial rate response. Am J Physiol - Hear Circ Physiol 256.

Bloom FE, Hoffer BJ, Siggins GR (1971) Studies on norepinephrine-containing afferents to Purkinje cells of rat cerebellum. I. Localization of the fibers and their synapses. Brain Res 25:501–521.

Bouret S, Sara SJ (2004) Reward expectation, orientation of attention and locus coeruleus-medial frontal cortex interplay during learning. Eur J Neurosci 20:791–802.

Carey MR, Regehr WG (2009) Noradrenergic Control of Associative Synaptic Plasticity by Selective Modulation of Instructive Signals. Neuron 62:112–122 Available at: http://dx.doi.org/10.1016/j.neuron.2009.02.022.

Carrasco M, Barbot A (2014) How attention affects spatial resolution. Cold Spring Harb Symp Quant Biol 79:149–160.

Carrasco M, Evert DL, Chang I, Katz SM (1995) The eccentricity effect: Target eccentricity affects performance on conjunction searches. Percept Psychophys 57:1241–1261.

Clewett D, Gasser C, Davachi L (2020) Pupil-linked arousal signals track the temporal organization of events in memory. Nat Commun 11:1–13.

Clewett D V., Huang R, Velasco R, Lee TH, Mather M (2018) Locus coeruleus activity strengthens prioritized memories under arousal. J Neurosci 38:1558–1574.

Corneil BD, Munoz DP (2014) Overt Responses during Covert Orienting. Neuron 82:1230–1243 Available at: http://dx.doi.org/10.1016/j.neuron.2014.05.040.

Danev SG, de Winter CR (1971) Heart rate deceleration after erroneous responses. Psychol Forsch 35:27–34.

Dawson ME, Schell AM, Filion DL (2007) The Electrodermal System. In: The Handbook of Psychophysiology, 3rd ed. (Cacioppo J, Tassinary LG, Bernston GG, eds), pp 159–181. Cambridge, MA, US: Cambridge University Press.

de Berker AO, Rutledge RB, Mathys C, Marshall L, Cross GF, Dolan RJ, Bestmann S (2016) Computations of uncertainty mediate acute stress responses in humans. Nat Commun 7:10996 Available at: http://www.pubmedcentral.nih.gov/articlerender.fcgi?artid=4820542&tool=pmcentrez&rendertype=abstract.

Donchin E, Coles MGH (1988) Is the P300 component a manifestation of context updating? Behav Brain Sci 11:357–427 Available at: https://www.researchgate.net/profile/Emanuel_Donchin/publication/232559111_Is_the_P300_component_a_manifestation_of_context_updating/links/55ef861108aef559dc44d610/Is-the-P300-component-a-manifestation-of-context-updating.pdf.

Fernandez-Ruiz J, Wong W, Armstrong IT, Flanagan JR (2011) Relation between reaction time and reach errors during visuomotor adaptation. Behav Brain Res 219:8–14 Available at: http://dx.doi.org/10.1016/j.bbr.2010.11.060.

Fine MS, Thoroughman KA (2006) Motor adaptation to single force pulses: Sensitive to direction but insensitive to within-movement pulse placement and magnitude. J Neurophysiol 96:710–720.

Gilzenrat MS, Nieuwenhuis S, Jepma M, Cohen JD, State RC (2010) Pupil diameter tracks changes in control state predicted by the adaptive gain theory of locus coeruleus function. Cogn Affect Behav Neurosci 10:252–269.

Gomi H, Kawato M (1996) Equilibrium-point control hypothesis examined by measured arm stiffness during multijoint movement. Science (80-) 272:117–120.

Gomi H, Kawato M (1997) Human arm stiffness and equilibrium-point trajectory during multi-joint movement. Biol Cybern 76:163–171.

Haith AM, Huberdeau DM, Krakauer JW (2015) The influence of movement preparation time on the expression of visuomotor learning and savings. J Neurosci 35:5109–5117.

Hayashi T, Kato Y, Nozaki D (2020) Divisively normalized integration of multisensory error information develops motor memories specific to vision and proprioception. J Neurosci 40:1560–1570.

Heald JB, Lengyel M, Wolpert DM (2023) Contextual inference in learning and memory. Trends Cogn Sci 27:43–64 Available at: https://doi.org/10.1016/j.tics.2022.10.004.

Hervé-Minvielle A, Sara SJ (1995) Rapid habituation of auditory responses of locus coeruleus cells in anaesthetized and awake rats. Neuroreport 6:1235–1240.

Huberdeau DM, Krakauer JW, Haith AM (2015) Dual-process decomposition in human sensorimotor adaptation. Curr Opin Neurobiol 33:71–77 Available at: http://dx.doi.org/10.1016/j.conb.2015.03.003.

Jepma M, Nieuwenhuis S (2011) Pupil diameter predicts changes in the exploration-exploitation trade-off: Evidence for the adaptive gain theory. J Cogn Neurosci 23:1587–1596.

Joshi S, Gold JI (2020) Pupil Size as a Window on Neural Substrates of Cognition. Trends Cogn Sci 24:466–480 Available at: https://doi.org/10.1016/j.tics.2020.03.005.

Joshi S, Li Y, Kalwani RM, Gold JI (2016) Relationships between Pupil Diameter and Neuronal Activity in the Locus Coeruleus , Colliculi , and Cingulate Cortex. Neuron 89:221–234 Available at: http://dx.doi.org/10.1016/j.neuron.2015.11.028.

Kagerer FA, Contreras-Vidal JL, Stelmach GE (1997) Adaptation to gradual as compared with sudden visuo-motor distortions. Exp Brain Res 115:557–561.

Kahneman D, Beatty J (1966) Pupil Diameter and Load on Memory. Science (80-) 154:1583–1585.

Kasuga S, Hirashima M, Nozaki D (2013) Simultaneous processing of information on multiple errors in visuomotor learning. PLoS One 8:e72741 Available at: http://www.pubmedcentral.nih.gov/articlerender.fcgi?artid=3756985&tool=pmcentrez&rendertype=abstract [Accessed September 24, 2014].

Krakauer JW, Hadjiosif AM, Xu J, Wong AL, Haith AM (2019) Motor learning. Compr Physiol 9:613–663.

Lenartowicz A, Escobedo-Quiroz R, Cohen JD (2010) Updating of context in working memory: An event-related potential study. Cogn Affect Behav Neurosci 10:298–315.

Makino Y, Hayashi T, Nozaki D (2023) Divisively normalized neuronal processing of uncertain visual feedback for visuomotor learning. Commun Biol 6:1–14.

Maresch J, Werner S, Donchin O (2021) Methods matter: Your measures of explicit and implicit processes in visuomotor adaptation affect your results. Eur J Neurosci 53:504–518.

Maris E, Oostenveld R (2007) Nonparametric statistical testing of EEG- and MEG-data. J Neurosci Methods 164:177–190.

Marko MK, Haith AM, Harran MD, Shadmehr R (2012) Sensitivity to prediction error in reach adaptation.

J Neurophysiol 108:1752–1763.

Mazzoni P, Krakauer JW (2006) An implicit plan overrides an explicit strategy during visuomotor adaptation. J Neurosci 26:3642–3645.

McBurney-Lin J, Vargova G, Garad M, Zagha E, Yang H (2022) The locus coeruleus mediates behavioral flexibility. Cell Rep 41:111534 Available at: https://doi.org/10.1016/j.celrep.2022.111534.

McDougle SD, Bond KM, Taylor JA (2015) Explicit and implicit processes constitute the fast and slow processes of sensorimotor learning. J Neurosci 35:9568–9579.

Miyamoto YR, Wang S, Smith MA (2020) Implicit adaptation compensates for erratic explicit strategy in human motor learning. Nat Neurosci 23:443–455 Available at: http://dx.doi.org/10.1038/s41593-020-0600-3.

Murphy PR, Robertson IH, Balsters JH, O'connell RG (2011) Pupillometry and P3 index the locus coeruleus-noradrenergic arousal function in humans. Psychophysiology 48:1532–1543 Available at: http://www.ncbi.nlm.nih.gov/pubmed/21762458 [Accessed September 7, 2014].

Murphy PR, Van Moort ML, Nieuwenhuis S (2016) The pupillary orienting response predicts adaptive behavioral adjustment after errors. PLoS One 11:1–11 Available at: http://dx.doi.org/10.1371/journal.pone.0151763.

Nassar MR, Rumsey KM, Wilson RC, Parikh K, Heasly B, Gold JI (2012) Rational regulation of learning dynamics by pupil-linked arousal systems. Nat Neurosci 15:1040–1046 Available at: http://dx.doi.org/10.1038/nn.3130.

Neville KM, Cressman EK (2018) The influence of awareness on explicit and implicit contributions to visuomotor adaptation over time. Exp Brain Res 236:2047–2059 Available at: http://dx.doi.org/10.1007/s00221-018-5282-7.

Ng GA, Brack KE, Coote JH (2001) Effects of direct sympathetic and vagus nerve stimulation on the physiology of the whole heart - A novel model of isolated Langendorff perfused rabbit heart with intact dual autonomic innervation. Exp Physiol 86:319–329.

Olson L, Fuxe K (1971) On the projections from the locus coeruleus noradrenaline neurons: The cerebellar innervation. Brain Res 28:165–171.

Palidis DJ, Cashaback XJGA, Gribble XPL (2019) Control of Movement Neural signatures of reward and sensory error feedback processing in motor learning. :1561–1574.

Palidis DJ, Gribble XPL (2020) Control of Movement EEG correlates of physical effort and reward processing during reinforcement learning. :610–622.

Poe GR, Foote S, Eschenko O, Johansen JP, Bouret S, Aston-Jones G, Harley CW, Manahan-Vaughan D, Weinshenker D, Valentino R, Berridge C, Chandler DJ, Waterhouse B, Sara SJ (2020) Locus coeruleus: a new look at the blue spot. Nat Rev Neurosci 21:644–659 Available at: http://dx.doi.org/10.1038/s41583-020-0360-9.

Polich J (2007) Updating P300 : An integrative theory of P3a and P3b. 118:2128–2148.

Preuschoff K, ’t Hart BM, Einhäuser W (2011) Pupil dilation signals surprise: Evidence for noradrenaline’s role in decision making. Front Neurosci 5:1–12.

Roelofs K, Dayan P (2022) Freezing revisited: coordinated autonomic and central optimization of threat coping. Nat Rev Neurosci 23:568–580.

Sakaguchi Y, Akashi Y, Takano M (2001) Visuo-Motor Adaptation to Stepwise and Gradual Changes in the Environment: Relationship between Consciousness and Adaptation. J Robot Mechatronics 13:601–613.

Sara SJ (2009) The locus coeruleus and noradrenergic modulation of cognition. Nat Rev Neurosci 10:211–223 Available at: http://www.ncbi.nlm.nih.gov/pubmed/19190638 [Accessed July 9, 2014].

Sara SJ, Bouret S (2012) Orienting and Reorienting : The Locus Coeruleus Mediates Cognition through Arousal. Neuron 76:130–141 Available at: http://dx.doi.org/10.1016/j.neuron.2012.09.011.

Sara SJ, Devauges V (1988) Priming stimulation of locus coeruleus facilitates memory retrieval in the rat. Brain Res 438:299–303.

Sara SJ, Roullet P, Przybyslawski J (1999) Consolidation of memory for odor-reward association: β-Adrenergic receptor involvement in the late phase. Learn Mem 6:88–96.

Scheidt RA, Reinkensmeyer DJ, Conditt MA, Zev Rymer W, Mussa-Ivaldi FA (2000) Persistence of motor adaptation during constrained, multi-joint, arm movements. J Neurophysiol 84:853–862.

Shadmehr R, Smith M a, Krakauer JW (2010) Error correction, sensory prediction, and adaptation in motor control. Annu Rev Neurosci 33:89–108 Available at: http://www.ncbi.nlm.nih.gov/pubmed/20367317 [Accessed November 8, 2013].

Strange BA, Hurlemann R, Dolan RJ (2003) An emotion-induced retrograde amnesia in humans is amygdala- and β-adrenergic-dependent. Proc Natl Acad Sci U S A 100:13626–13631.

Sun N, Li BX, Hong YJ, Bing YH, Qiu DL, Chu CP (2019) Noradrenaline depresses spontaneous complex spikes activity of cerebellar Purkinje cells via α2-adrenergic receptor in vivo in mice. Neurosci Lett 703:38–44 Available at: https://doi.org/10.1016/j.neulet.2019.03.008.

Szabadi E (2013) Functional neuroanatomy of the central noradrenergic system. J Psychopharmacol 27:659–693.

Takeuchi T, Duszkiewicz AJ, Sonneborn A, Spooner PA, Yamasaki M, Morris RGM, Watanabe M, Smith CC, Fernández G, Deisseroth K, Robert W (2016) Locus coeruleus and dopaminergic consolidation of everyday memory. Nature 537:357–362 Available at: http://dx.doi.org/10.1038/nature19325.

Taylor JA, Thoroughman KA (2007) Divided attention impairs human motor adaptation but not feedback control. J Neurophysiol 98:317–326.

Taylor JA, Thoroughman KA (2008) Motor Adaptation Scaled by the Difficulty of a Secondary Cognitive Task. 3.

Tsay JS, Kim HE, McDougle SD, Taylor JA, Haith A, Avraham G, Krakauer JW, Collins AGE, Ivry RB (2024) Fundamental processes in sensorimotor learning: Reasoning, refinement, and retrieval. Elife

13:1–25.

van der Molen MW, Boomsma DI, Jennings JR, Nieuwboer RT (1989) Does the heart know what the eye sees? A cardiac/pupillometric analysis of motor preparation and response execution. Psychophysiology 26:70–80.

Vankov A, Hervé-Minvielle A, Sara SJ (1995) Response to Novelty and its Rapid Habituation in Locus Coeruleus Neurons of the Freely Exploring Rat. Eur J Neurosci 7:1180–1187.

Vinzi VE, Chin WW, Henseler J, Wang H (2010) Handbook of Partial Least Squares Concept, Methods and Applications (Vinzi VE, Chin WW, Henseler J, Wang H, eds). Springer.

Wakita R, Tanabe S, Tabei K, Funaki A, Inoshita T, Hirano T (2017) Differential regulations of vestibulo-ocular reflex and optokinetic response by β - and α 2-adrenergic receptors in the cerebellar flocculus. :1–12.

Walsh MM, Anderson JR (2012) Learning from experience: Event-related potential correlates of reward processing, neural adaptation, and behavioral choice. Neurosci Biobehav Rev 36:1870–1884 Available at: http://dx.doi.org/10.1016/j.neubiorev.2012.05.008.

Wang CA, Munoz DP (2015) A circuit for pupil orienting responses: Implications for cognitive modulation of pupil size. Curr Opin Neurobiol 33:134–140 Available at: http://dx.doi.org/10.1016/j.conb.2015.03.018.

Wei K, Körding K (2009) Relevance of error: What drives motor adaptation? J Neurophysiol 101:655–664.

Werner S, Van Aken BC, Hulst T, Frens MA, Van Der Geest JN, Strüder HK, Donchin O (2015) Awareness of sensorimotor adaptation to visual rotations of different size. PLoS One 10:1–18.

White O, French RM (2016) Pupil Diameter May Reflect Motor Control and Learning. 2895.

Wolpert DM, Diedrichsen J, Flanagan JR (2011) Principles of sensorimotor learning. Nat Rev Neurosci 12:739–751 Available at: http://dx.doi.org/10.1038/nrn3112.

Yokoi A, Weiler J (2022) Pupil diameter tracked during motor adaptation in humans. J Neurophysiol 128:1224–1243.

Zhang Z, Wang H, Zhang T, Nie Z, Wei K (2024) Perceptual error based on Bayesian cue combination drives implicit motor adaptation. Elife 13.